Scientific Research Publishing

Materials Sciences and Applications, 2026, 17(2), 50-66
https://www.scirp.org/journal/msa
ISSN Online: 2153-1188
ISSN Print: 2153-117X

Generation of Reactive Oxygen Species (ROS) on the Surface of Severe Plastically Deformed Pure Copper Processed by High-Pressure Torsion (HPT)

Ken Hirota[1*], Kento Kominami[2], Aoi Horinouchi[2], Kazuhiko Tsukagoshi[1,2], Hiroshi Kawakami[3], Kaveh Edalati[4], Takashi Ozawa[5]

[1]Research Center of Bio-Micro-Fluidic Science, Doshisha University, Kyoto, Japan
[2]Department of Chemical Engineering and Materials Science, Faculty of Science & Engineering, Doshisha University, Kyoto, Japan
[3]Graduate School of Engineering, Osaka Metropolitan University, Osaka, Japan
[4]International Institute for Carbon-Neutral Energy Research (I2CNER), Kyushu University, Fukuoka, Japan
[5]Japan Copper Development Association, Tokyo, Japan
Email: *khirota@mail.doshisha.ac.jp

How to cite this paper: Hirota, K., Kominami, K., Horinouchi, A., Tsukagoshi, K., Kawakami, H., Edalati, K. and Ozawa, T. (2026) Generation of Reactive Oxygen Species (ROS) on the Surface of Severe Plastically Deformed Pure Copper Processed by High-Pressure Torsion (HPT). *Materials Sciences and Applications*, **17**, 50-66.
https://doi.org/10.4236/msa.2026.172004

Received: December 30, 2025
Accepted: February 6, 2026
Published: February 9, 2026

Abstract

To investigate the antibacterial activity of severe plastically deformed pure Cu by high-pressure torsion (HPT), the generation of reactive oxygen species (ROS) which might be the main origin of antibacterial activity of Cu, Cu disc (1.00×10^{-2} m in diameter, 1.0×10^{-3} m thick) has been evaluated using chemiluminescence (CL) with the luminol solution; HPT processes were performed under various torsion turns, 0, 1/4, 1, 3 and 10 turns under uniaxial pressure of 6.0 GPa and rotating speed of 1.667/s (1.0 rpm) at room temperature. Cu disc which was HPT-processed with the 1/4 turn, simply denoted as $HPT_{1/4}$ Cu disc, showed the highest summation of CL intensity, ΣCL, among those of other HPTed discs, and this value was 2.7 times higher than that of as-obtained disc. Furthermore, $HPT_{1/4}$ disc heated at 523 K (250˚C) in a vacuum (2×10^{-3} Pa) for 1.8×10^{3} s (30 min) brought much higher ΣCL value, about 35 times of as-obtained disc. Then, the components of ROS generated were investigated using the combination of luminol + scavengers corresponding to each ROS. About 45% of ROS were strong antibacterial active hydroxy radical ·OH and hydrogen peroxide H_2O_2.

Keywords

Copper, High-Pressure Torsion, Antibacterial Activity, Reactive Oxygen Species, Chemiluminescence

1. Introduction

As exhibiting both prominent ductility and tractility, copper is a suitable metal material for plastic deformation processing such as i) forging [1], ii) rolling [2], iii) stamping [3], iv) extrusion [4], v) drawing [5], and vi) forming [6]. In general, it has been told that much strain which has been introduced by plastic deformation often induces degradation of mechanical properties [7]. However, recently, ultra-large strain processing [8] has been attracting due to a new finding of much improvement or change of mechanical [9], electrical/electronic [10], and thermal properties [11] which have been brought by the change in its micro- or nano-structure. Severe plastic deformation is one of the most effective approach to control micro- or nano-structure. There are different kinds of severe plastic deformation processing, such as equal-channel angular pressing (ECAP) [10], high-pressure sliding (HPS) [12], and high-pressure torsion (HPT) [13]. Many papers on the mentioned properties of severe-plastic-deformation-processed pure Cu have been published [14]. For example, the microstructure and mechanical properties of Cu processed by HPT were investigated [9]. Furthermore, the evolution of electrical conductivity and hardness with strain has been evaluated for ECAP and HPT processed Cu [15].

The present authors have been studying the antibacterial activities of metal oxide powders, ZnO [16] and rutile TiO_2 [17] using chemical luminescence (CL) [18], and developed the significant antibacterial ZnO and TiO_2 which reveal continuous antimicrobial activity even under light shielding. Recently, we have changed the studying materials from metal oxide to pure metal, especially, focused on copper because Cu has been widely recognized as antibacterial material [19]. As the antibacterial activity is much dependent on the physical and chemical properties of outermost surfaces, it requires analytical technology for the evaluation of surface, in addition to the conventional analyzing techniques to study the mechanism of antibacterial activity. Due to large surface area compared with bulk, the fine powder was selected first for studying antibacterial activity of Cu [20]. We studied and found the good powder additives (anatase TiO_2) [20] to enhance its antimicrobial activity of powder Cu. Then, we focused on investigating the thermal effect on the antibiotic properties bulk Cu, which resulted in finding a suitable heat treatment to introduce the formation of Cu oxides, such as Cu_2O and CuO thin films on the surface of Cu [21]. Then, the relationship between crystal plane and antibacterial activity was studied [22]; it was found that (100) plane was dominant for improving the antimicrobial activity of Cu. Furthermore, we have changed our study from basic science to industrial technology *i.e.*, investigating the relationship between the plastic deformation and antibacterial activity; because up to now few papers concerning about this subject have been published, nevertheless their mechanical properties have been much investigated. To study the antibacterial activity of plastically deformed pure Cu, the generation of reactive oxygen species (ROS) on the surface Cu has been evaluated [18]. Here, it should be clarified that it has been already reported that ROS has a strong rela-

tionship on killing bacteria and virus proved by using Escherichia coli (E. coli), Staphylococcus aureus (S. aureus) and A/Hong Kong virus [22].

In the present study, high-pressure torsion (HPT) was used as the plastic deformation process to give the sever controlled deformation to Cu test piece. And the generation of ROS was thought to be occurred on the outermost surface consisting of nanometer size thin-films of Cu_2O/CuO on bulk Cu, a chemiluminescence (CL) method with luminol aqueous solution was adopted because this technique is very sensitive to detect ROS, furthermore, among four kinds of ROS; hydroxy radical ·OH, hydrogen peroxide H_2O_2, superoxide anion $\cdot O_2^-$ and singlet oxygen $^1O_2$, to determine which ROS is mainly generated, the CL with the combination of luminol and scavengers [23] corresponding to each ROS was also adopted.

The purpose of this study is to evaluate the intensity change in antimicrobial activity of severely deformed pure Cu and to clarify the relationship between antimicrobial activity and deformation of Cu.

2. Experimental Procedure

2.1. Sample Preparation of Severe Plastically Deformed Pure Cu Discs and Test Pieces for Chemiluminescence Evaluation

Oxygen-free copper (99.99% purity, C1020) discs with diameter 1.00×10^{-2} m, thickness 1.0×10^{-3} m (Kikukawa Industry Co. Ltd, Tokyo, Japan) was used as starting material. These Cu discs were severe plastically deformed by high-pressure torsion (HPT) apparatus, under a 6 GPa vertical pressure, torsion turns of 0, 1/4, 1.0, 3.0 and 10, a rotating speed of 1.667×10^{-2} /s (1.0 rpm: round per minute) at room temperature (R.T.). As far as torsion processing, the upper portion of Cu disc was fixed by the upper anvil and the bottom of disc was rotated by the lower anvil. The surfaces of both upper and lower anvils contacted with the Cu disc were consisted of concavity/convexity squares with a one side length of 175 μm and 40 μm in depth. After the various HPT processing, Cu discs were heated under vacuum using the combined rotary and diffusion pumps (a degree of vacuum: 2.0×10^{-3} Pa) with the rotary & diffusion pumps at 423 to 573 K for 1.8×10^3 s; these conditions were determined as follows: i) the degree of vacuum; 2.0×10^{-4} Pa, 2.0×10^{-3} Pa, 2.0×10^{-1} Pa, ii) heating temperatures; 423 K, 473 K, 523 K, 573 K, and iii) soaking time; 6.0×10^2 s, 1.8×10^3 s, 6.0×10^3 s, and 1.8×10^3 s were examined. Among them, the vacuum heating conditions of 2.0×10^{-3} Pa, 523 K, 1.8×10^3 s gave the highest ΣCL value as mentioned afterward.

To evaluate the depth profile of chemiluminescence intensity, the Cu disc samples were grinded with #1000 mesh SiC powders immersed in machine oil not to be oxidized during polishing.

2.2. Evaluation

2.2.1. Physicochemical Property

The thickness of Cu discs was measured using a digital micrometer. Powder X-ray diffraction (XRD: Smartlab, Rigaku, Tokyo, Japan) analysis with Cu*Kα* radia-

tion (a wavelength of 0.15418 nm) was utilized for identification of the crystalline phases and evaluation of both crystallite sizes X_s and a lattice parameter ***a*** of Cu, and grain orientation Q (HKL) for crystal plane (HKL) using the following equation; Q (HKL) = [ΣI (HKL)/ΣI (hkl)] × 100 (%). Here, ΣI (HKL) is the summation of (HKL) plane's diffraction intensity I (HKL), and ΣI (hkl) is the summation of all (hkl) plane's diffraction intensities I (hkl). However, as the crystal structure of Cu is face-centered cubic (FCC) and due to the extinction law, ΣI (HKL) is only I (200); however, ΣI (hkl) is I (111) + I (200) + I (220) + I (311). The measuring conditions for both powder and thin-film XRDs were the same as follows: accelerating electric voltage and current were 45 kV and 200 mA, respectively, a scanning speed 1.667×10^{-1}˚/s (10˚/min) with a 0.01˚/step, a scanning angle 2 θ: 15˚ - 100˚, except for an incident angle of 0.5˚ and a scanning speed 1.667×10^{-2}˚/s (1˚/min) for the latter.

Surface aspect and roughness of Cu discs were studied using a laser microscope (VK-X100/X200, Keyence, Osaka, Japan). Microstructural observation with a field emission-type scanning electron microscope (FE-SEM; SU8020, acceleration voltage 15 kV, Hitachi High-Technologies Corporation, Tokyo, Japan).

2.2.2. Chemiluminescence (CL) Intensity Measurement and Evaluation of Reactive Oxygen Species (ROS)

Chemiluminescence (CL) of Cu discs in a 2.5×10^{-7} m^3 (0.25 mL) aqueous luminol solution with a concentration of 5.0×10^{-1} - 5.0×10^{-2} mol × m^{-3} (5.0×10^{-4} - 5.0×10^{-5} mol × L^{-1}) mixed with 4.0×10^{-6} m^3 (4.0 mL) carbonic acid buffer solution ($NaOH/NaHCO_3$, pH = 10.8 - 10.9) [24] was observed under dark conditions using a CL detector (CLA-FS3, Tohoku Electronic Industrial Co., Ltd., Sendai, Japan). After dropping the luminol solution in a 6.0×10^1 s' warming up of the detector, the intensity of CL was integrated between 6.1×10^1 - 6.0×10^2 s. The summation of CL intensity for 5.4×10^2 s (9 min), ΣCL (9 min), which was calculated as follows: at first, estimate the summation of background noise, ΣCL (BG), from 0 to 6.0×10^1 s, and then summarize the CL intensity from 6.1×10^1 to 6.0×10^2 s, ΣCL (total 9 min), finally, the true ΣCL (9 min) was determined to be ΣCL (total 9 min) – ΣCL (BG) × 9. This true ΣCL (9 min), in a simple term, ΣCL (9 min) value was utilized to evaluate the amount of ROS generated from the surface of Cu disc.

To determine 4 kind of ROS [25] shown in **Table 1**, hydroxy radical ·OH, hydrogen peroxide H_2O_2, superoxide anion $\cdot O_2^-$, and singlet oxygen $^1O_2$, scavengers [23], 2-propanol ("2-pro", for ·OH, Nacalai Tesque Chemicals, Kyoto, Japan), sodium pyruvate ("s-pyr", for H_2O_2, Fuji-film Wako Pure Chemical Co., Ltd., Osaka, Japan), nitro blue tetrazolium ("nbt", for $\cdot O_2^-$, Nacalai Tesque Chemicals) and sodium azide (for short "NaN_3", for $^1O_2$, Fuji-film Wako Pure Chemical) were used to determine which ROS was generated. At first, these scavengers were solved into the buffer solution with the concentration 5.0×10^{-2} mol × m^{-3} (5.0×10^{-5} mol × L^{-1}). Both each solution and a 4.0×10^{-6} m^{-3} (4.0 mL) pure buffer solution was mixed. CL measurement was performed as the same as CL intensity measure-

ment, after a 6.0×10^1 s' warming up of the detector, the intensity of CL was integrated between 6.0×10^1 - 6.0×10^2 s. The amount of difference (D) for each ROS was evaluated using the equation of D = ΣCL (9 min, without scavenger) – ΣCL (9 min, with scavenger).

Table 1. Reactive oxygen species (ROS) and corresponding scavengers.

ROS		Scavengers
·OH	Hydroxy radical	2-propanol (2-pro)
H_2O_2	Hydrogen peroxide	Sodium pyruvate (s-pyr)
$\cdot O_2^-$	Superoxide anion	Nitroblue tetrazolium (nbt)
$^1O_2$	Singlet oxygen	Sodium azide (NaN3)

3. Results and Discussion

3.1. Physical Properties, Such as Thickness and Crystal Structures of Cu Discs

Figure 1 shows the compression rates t/t_o of Cu discs prepared by HPT process (under 6.0 GPa with the rotating speed of 1.0 rpm) as a function of number of HPT rotations. From 0 to 1/4 rotation, thickness ***t*** is decreased rapidly, compression rate t/t_o is also down to 71% - 76%, and after 1 rotation ***t*** is reduced gradually up to 10 rotation; there, compression rates t/t_o is reached at around 64%.

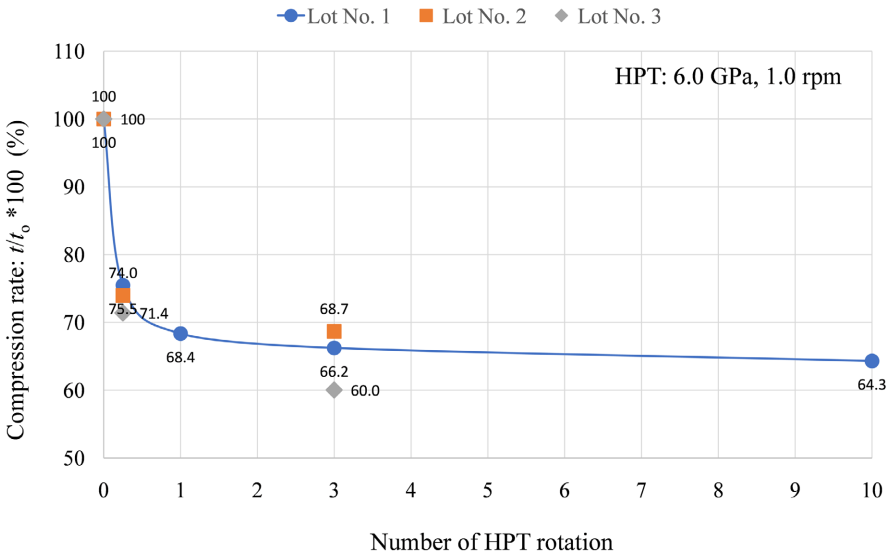

Figure 1. Compression rates t/t_o of various Cu discs prepared by HPT.

Figure 2 shows the powder X-ray diffraction (XRD) patterns of Cu surfaces of (a) as-obtained and (b) after HPT 1/4 rotation, respectively, afterward abbreviated $HPT_{1/4}$ is used. Much difference between them is the XRD intensities of I (111) and I (200); I (200) is the highest among all diffraction peaks in the former (a),

however, instead of I (200), I (111) becomes the highest in the latter (b). It might be stated that the crystal plane (111) of slip surface of FCC [26] Cu becomes superior just after only 1/4 turn.

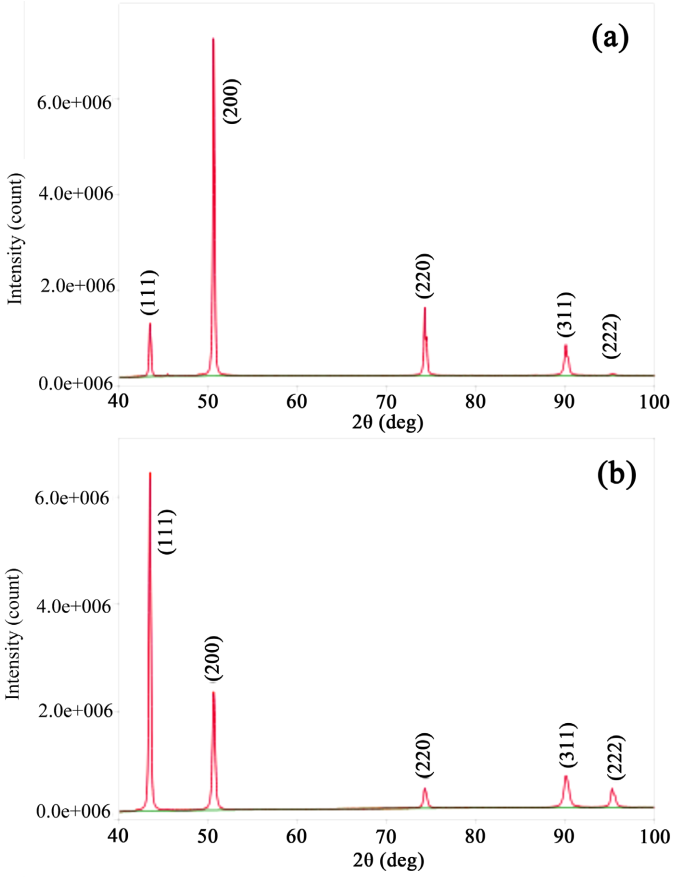

Figure 2. XRD patterns of (a) as-obtained Cu disc and (b) HPTed Cu disc after 1/4 turns.

Orientation degrees of (100) and (111) planes, denoted as Q (100) and Q (111), which were evaluated using the equations explained previously, of all severe plastic deformed Cu disc surfaces, were shown in **Figure 3**. A curve of decreasing Q (100) resembles the compression rate of Cu presented in **Figure 1**. Between as-obtained and $HPT_{1/4}$, *i.e.*, the numbers of HPT rotation are "0" and "0.25", Q (100) decrease rapidly and then gradually after HPT "1.0", followed by the passing through the lowest value of 17.2 and recovering to 20.4. On the contrary, Q (111) increases with increasing torsion turns rapidly between "0" and "0.25"and then gradually saturated, reversing the Q (100) curve. Then in order to recognize the change in microstructure of Cu discs, the crystallite size X_s of each crystal plane was evaluated using Scherre's equation [27] as shown in **Figure 4**. As-expected from **Figure 3**, between 0 and 1/4 (=0.25) number of HPT rotation, X_s of (200) crystal plane decreased much from 55.3 to 30.0 nm down to 54%. However, after 1/4 all X_s were recovered, especially X_s of (111) plane increased gradually than that of the as-obtained Cu disc, suggesting that severe plastic deformation induced the

crystalline growth of (111) plane; on the contrary, the crystallite sizes of other planes were almost constant. By the way, the angle between (100) and (111) planes is 54.7˚ in FCC structure [28].

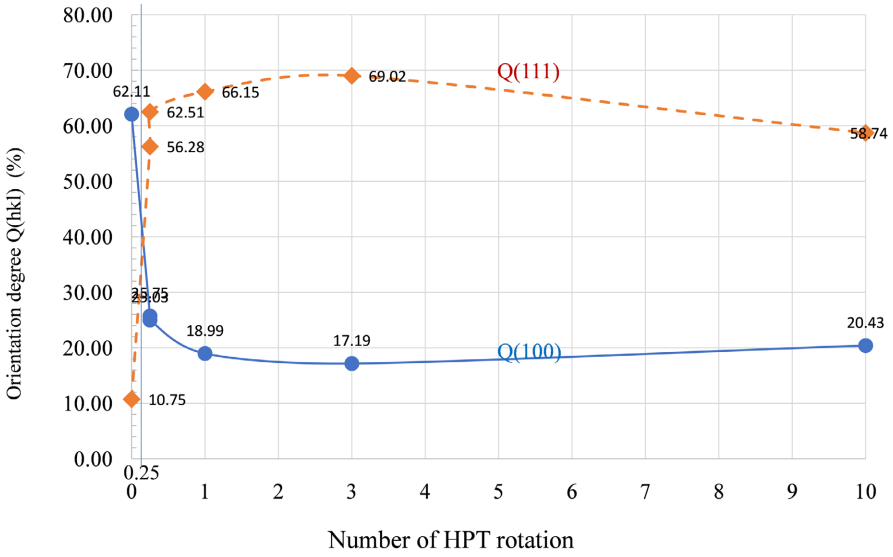

Figure 3. Orientation degrees Q (100) and Q (111) as a function of numbers of HPT rotation.

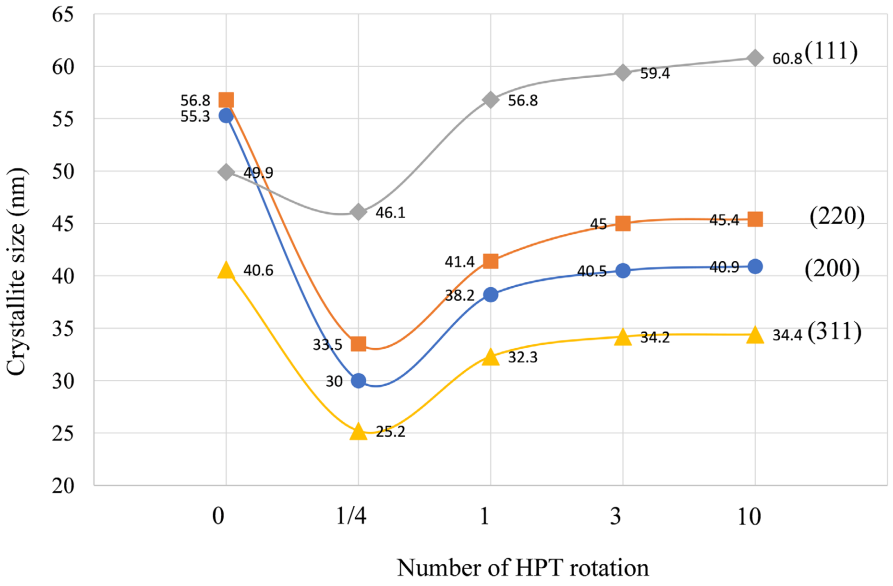

Figure 4. Crystallite sizes X_s determined by Scherre's-eq. as a function of numbers of HPT rotation.

3.2. Chemiluminescence (CL) of Cu Discs

In order to evaluate the antibacterial activity of Cu discs before and after HPT process, CL values were measured using luminescent luminol as described in 2.2.2. **Figure 5** shows the summation of CL intensity ΣCL (9 min) of Cu discs before and after HPT process, with that of Cu square plate ($25 \times 25 \times 1 \times 10^{-3}$ m in size) as a reference; this Cu plate was used in our previous experiment and reported [20]. As far as

ΣCL (9 min) values, its standard deviation was about 20 - 24 k·count, sample sizes (N) of all ΣCL (9 min) values were 5; among them, and the maximum and minimum values were deleted and the average value was calculated from three values. Only the average values were plotted as the representative points. As mentioned above **Figure 3**, a little (100) orientation for Cu disc (diameter 10, thickness 1.0×10^{-3} m in size), ΣCL (9 min) value is much higher than that of Cu plate nevertheless its smaller surface area. It should be noted that just after 1/4 rotation, $HPT_{1/4}$, ΣCL (9 min) values of both up and down sides surfaces become 2.0 to 2.7 times higher than that (1544 k·count) of as-obtained Cu. However, with increasing HPT rotation, ΣCL (9 min) declined gradually as resembling both orientation degree Q (111) and crystallite size X_s (111) inversely. Then, the relationship between ΣCL (9 min) and average strain ε was studied: the latter **e** was calculated using $\varepsilon = \langle r \rangle \times \theta \, \boldsymbol{t}/\sqrt{3}$ equation; here, $\langle r \rangle$ is average radius 3.53×10^{-3} m, θ rotation angle (radian), ***t*** thickness of Cu disc 1×10^{-3} m. **Figure 6** exhibits ΣCL (9 min) of Cu discs as a function of average strain ε, suggesting that there is much strong relationship between them; only small strain induced under high pressure can bring high ΣCL (9 min) value.

Based on some information that a vacuum heating had much influence on the ΣCL (9 min) of Cu thin film [22], $HPT_{1/4}$ and $HPT_{3.0}$ Cu discs were heated under vacuum (2×10^{-3} Pa) for 1.8×10^3 s (30 min). **Figure 7** shows ΣCL of various Cu discs of $HPT_{1/4}$ and $HPT_{3.0}$ as a function of vacuum heating temperature. Although $HPT_{3.0}$ reveals the highest ΣCL value of 2339 k·count at 523 K, $HPT_{1/4}$ presented the extremely high ΣCL value of 54,165 k·count after DP (Diffusion Pump) vacuum heating at the same temperature. The reason for this effect might be explained by "Passive film [29]". It has been reported that the higher stability of the Cu_2O (111) precursor formed on the Cu substrate in basic aqueous solution (0.1 M NaOH) in the initial stage of growth of the Cu (I)/Cu (II) duplex passive film

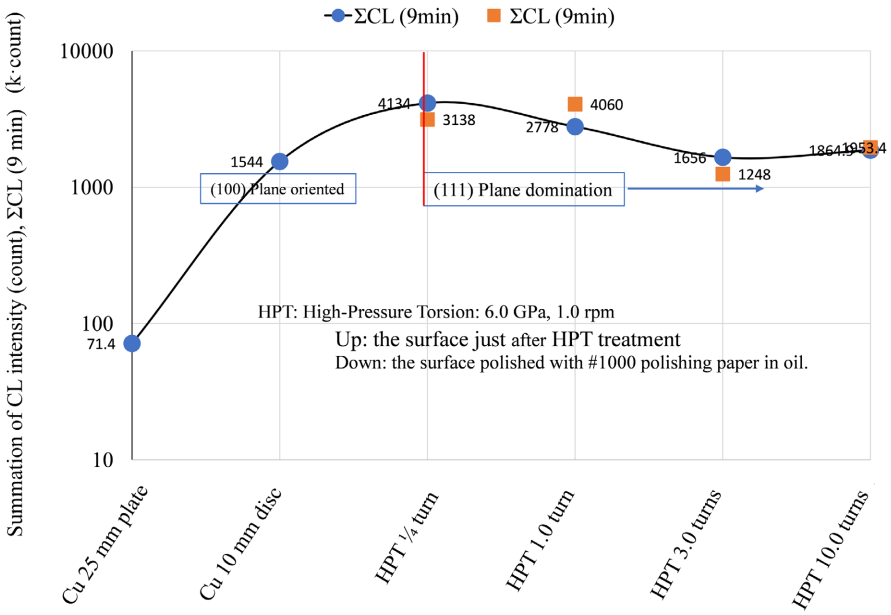

Figure 5. Summation of CL intensity ΣCL (9 min) of HPTed Cu discs.

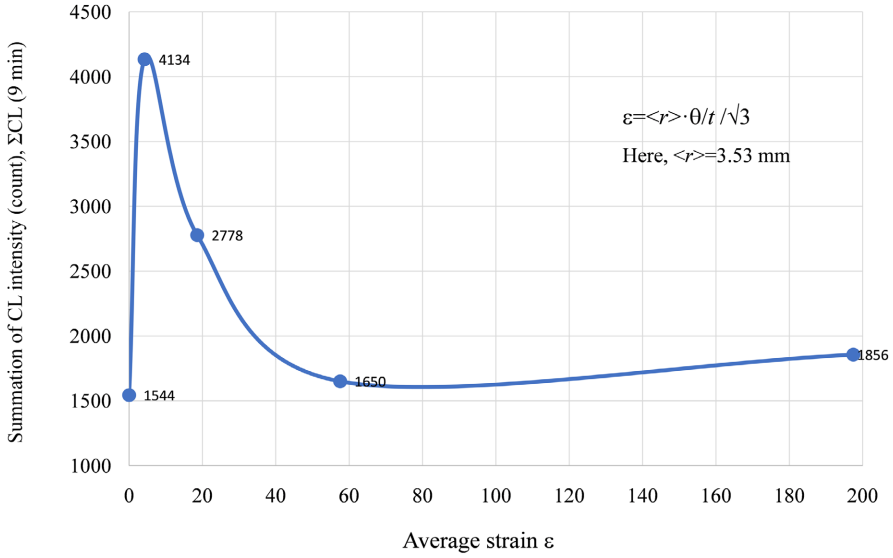

Figure 6. Summation of CL intensity ΣCL (9 min) of HPTed Cu disc *vs.* average strain *ε*.

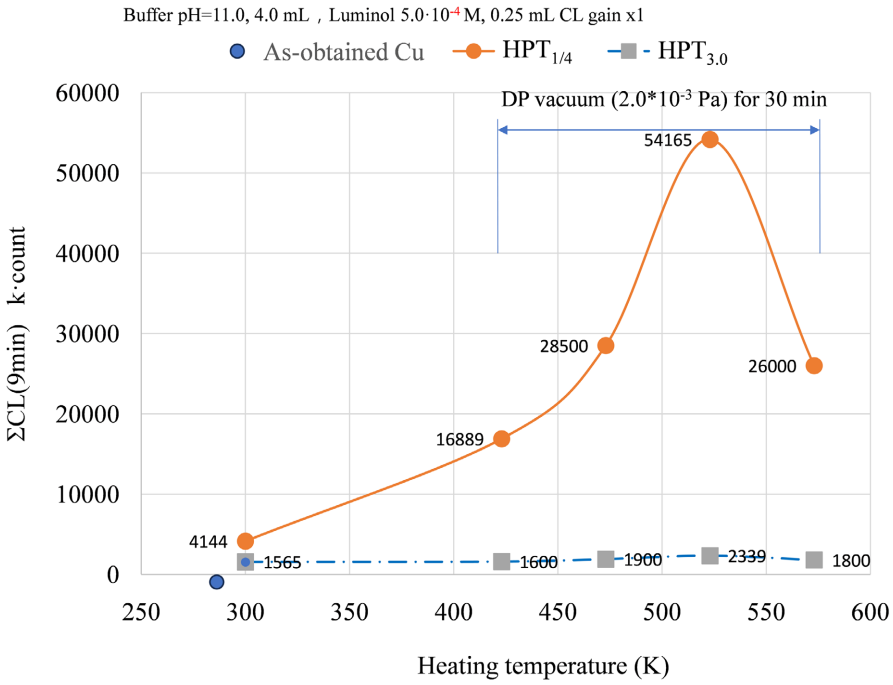

Figure 7. ΣCL of various Cu discs as a function of vacuum heating temperatures.

which could bring the generation of CuO/Cu_2O terrace or steps on the purified outermost surface of Cu, *i.e.*, many tiny CuO/Cu_2O thin-film oxide islands are formed at the most active edges [30] on the surface of Cu under low partial oxygen pressure (vacuum heating). These oxide islands formed on Cu surface after the vacuum heating were observed by the present authors using a high-resolution transmission electron microscope (TEM) [22].

Next the components of ROS were determined as the same methods as our previous reports [18] [20]. **Figure 8** summarized the CL intensity, where ΣCL (9 min)

values were presented as the height of bar graph and the components of ROS were color-coded in each bar. It should be noted that ΣCL of $HPT_{1/4}$ Cu disc increased 2.7 times higher than as-obtained disc, furthermore, a vacuum heating at 523 K for1.8×10^3 s (30 min) brought much higher ΣCL, about 35 times of that of as-obtained. And using the scavenger corresponding to each ROS, about 45% of ROS were strong antibacterial active hydroxy radical ·OH and hydrogen peroxide H_2O_2 [31].

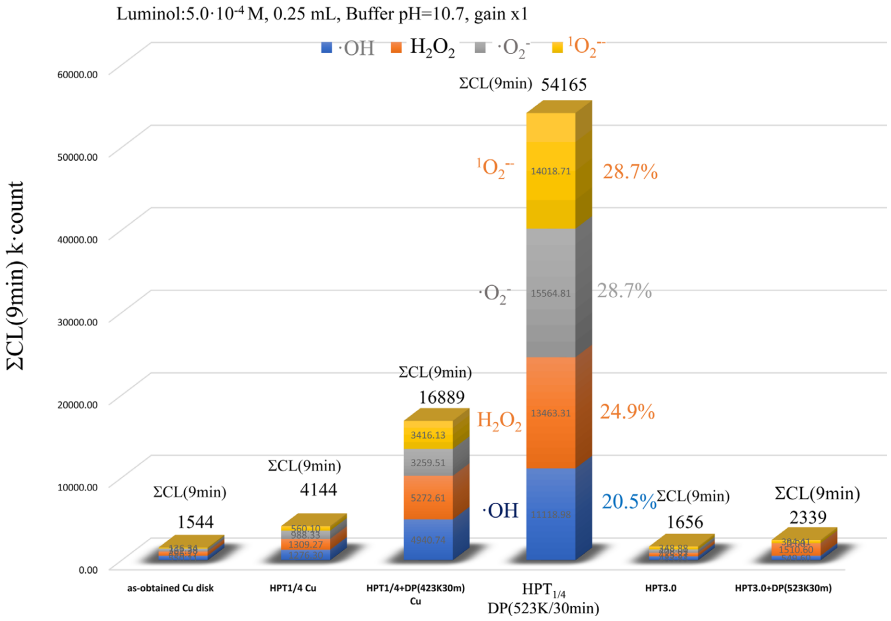

Figure 8. Components of ROS of various Cu discs.

3.3. Characterization of the Outermost Surface of Cu Discs

As it might be presumable that ROS could be generated on the outermost surface of Cu discs, the characterization of outermost surfaces of various Cu discs was performed. **Figure 9** shows the laser micrographs of the overview of as-obtained (A, top) and $HPT_{1/4}$ (B, top) with the line-analysis (intersect) (A, lower) and (B, lower), respectively, indicating roughness R_Z. Though the surface of as-obtained is relatively flat, that of $HPT_{1/4}$ consists of the concavity and convexity; a square on a side of 1.75×10^{-4} m (175 μm) with the height of about 4.0×10^{-5} m (40 μm). These squares were formed by the grip-surface of anvil during HPT process. Then, the outermost surfaces of as-obtained, $HPT_{1/4}$, and $HPT_{1/4}$ plus DP (diffusion pump vacuum 2.0×10^{-3} Pa/1.8×10^3 s/523 K) heating were observed using SEM under various magnifications. **Figure 10** exhibit their SEM images; top line (A-1, B-1, C-1), middle line (A-2, B-2, C-2), and bottom line (A-3, B-3, C-3), taken under low ($\times 10^2$), middle ($\times 10^3$), and high ($\times 10^4$) magnifications, respectively. On the contrary, the vertical line, left to right No.1 is as-obtained Cu, No. 2 $HPT_{1/4}$ Cu, and No. 3 $HPT_{1/4}$ plus DP Cu, images are presented. The values of ΣCL (9 min) and orientations of Q (100)/Q (111) are also shown in low and high magnifications lines, respectively. First of all, we noticed that when B-1 is compared with C-1, the surface of latter looks like being covered with "thin fog", as the same as B2 *vs.*C-2

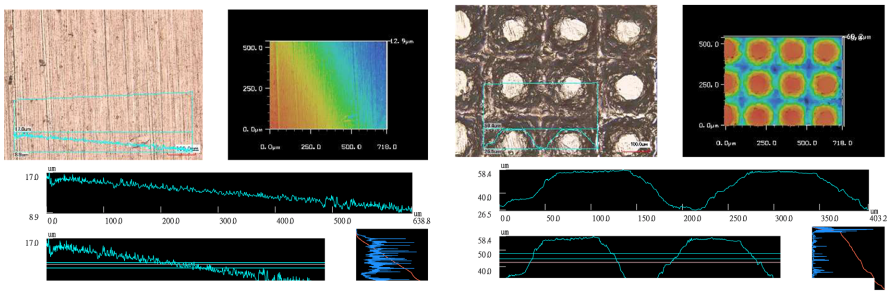

(A) Overview of as-obtained Cu disc with R_z (B) Overview of HPT$_{1/4}$ Cu disc with R_z

Figure 9. Laser micrographs of as-obtained and HPTed Cu discs with surface roughness information. (A) Overview of as-obtained Cu disc with R_z. (B) Overview of HPT$_{1/4}$ Cu disc with R_z.

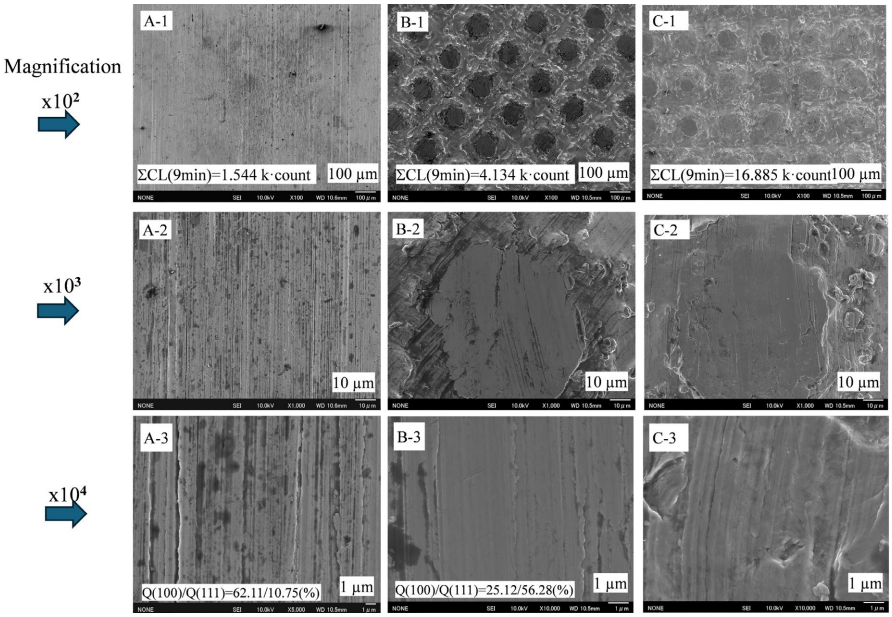

Figure 10. SEM photographs of the surface of Cu discs taken under various magnifications; (A) and (B) are as-obtained and prepared after HPT 1/4 process, respectively. (C) is prepared by vacuum heating (2.0×10^{-3}Pa for 30 min) at 523 K after HPT$_{1/4}$.

and B-3 *vs.* C-3, indicating the thin oxide film was generated on the outermost surface. In general, the formation of metal oxide thin-film on bulk metal in a vacuum has been explained as that two kinds of oxidation might be occurred; one is "Passive oxidation" [29] and the other is "Active oxidation" [29]. During the vacuum heating under 2.0×10^{-3} Pa ($P_{O2} = 4.2 \times 10^{-4}$ Pa) at 523 K, "passive oxidation" might occur; at first the absorbed water on the surface of HPT$_{1/4}$-Cu was removed, and then, thin-film of Cu_2O was formed under low partial oxygen pressure $P_{O2} = 4.2 \times 10^{-4}$ Pa near the active crystallite, grain boundaries and some crystal defects (voids, dislocations). At this temperature and P_{O2}, an equilibrium oxygen pressure-temperature reported for Cu [32] supports that CuO is stable. However, Cu_2O should have been generated on the outermost surface of Cu first, then thin-film of CuO was introduced on the Cu_2O layer. As mentioned above ROS could be gener-

ated mainly at the active steps [30] or edges between Cu_2O and CuO thin-films. Then, from the crystal viewpoint, the characterization has been performed to understand the relationship between the Cu crystallite changes and ΣCL.

Figure 11 shows thin-film XRD patterns of various Cu discs: as-obtained, upper and lower surfaces of $HPT_{1/4}$, and upper and lower surfaces of $HPT_{1/4}$ + 423 K/30 min vacuum heated. Although XRD patterns of all as-obtained and **upper** surfaces of $HPT_{1/4}$ and $HPT_{1/4}$ + 423 K/30 min DP vacuum heated are the same as Cu reported [33], those of **lower** surfaces of $HPT_{1/4}$ and $HPT_{1/4}$ + 423 K/30 min DP are a little different; all diffraction peaks are shifted to the higher angle, which means that the lattice constant of lower surface of Cu is smaller than ordinary Cu. This phenomenon can be explained by that the outermost surface (its depth might be estimated to be around 200 nm) [34] of lower surface was compressed in a horizontal direction during HPT process because the lower anvil was rotated, on the other hand, the upper anvil was immobilized. Based on these data the lattice constants ***a*** of upper and lower surfaces is calculated to be 0.35734 and 0.35320 nm, respectively. Here, it should be noted that the value of *a* (upper) is the same as a reported for bulk Cu [33]. Therefore, shear strain $\gamma = \Delta a/a$ (upper) = 0.00414, and transverse modulus *G* of copper is around 44.82 GPa [35], and then shear stress τ can be estimated to be around 0.52 GPa using an equation of $\tau = \gamma \cdot G$. This value is less than 1/10 of vertical stress 6.0 GPa. Here, it is noteworthy that the lower surface of Cu disc was much affected by shear stress than the upper surface.

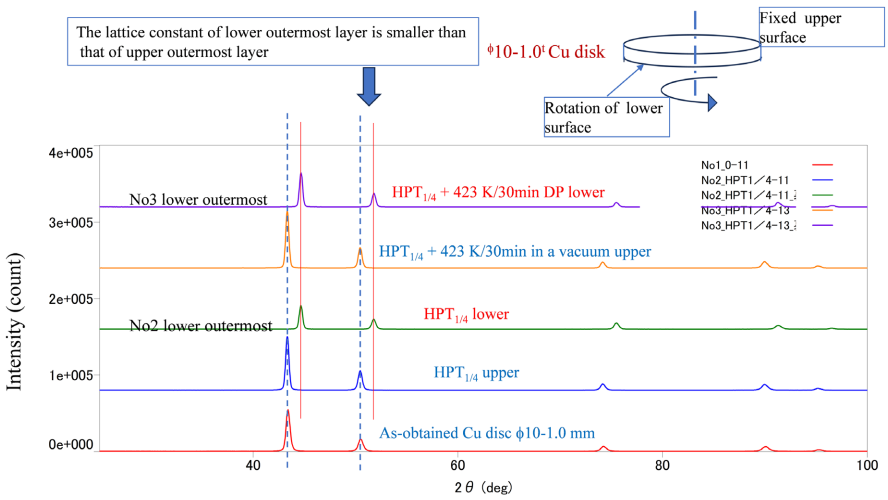

$HPT_{1/4}$ -DP 423 K/30min:*a* = 0.35734 (upper surface) and *a* =0. 35320 nm (lower surface).

Figure 11. Thin-film XRD patterns of various Cu discs: XRD patterns of both $HPT_{4/1}$ and + 423 K/30 min DP (vacuum heated), upper and lower surfaces.

Then the microstructural change in Cu disc before and after HPT process was studied. Figure 12 summarizes the orientation degrees Q (100), Q (111) and crystallite sizes X_s at the outermost and a few micron inside of as-obtained and $HPT_{1/4}$-Cu discs. The former (the outermost) and the latter (several tens of μm inside) were evaluated with thin-film and powder XRD analyses, respectively. At the

outermost surface of as-obtained Cu, the slipping surface of (111) plane [26] is dominant and on the contrary (100) plane is backfoot, followed by a small their X_s; this might be due to the production of metallic rolling process of Cu sheet with a 1.0 mm thickness. However, in the crystal structure of as-obtained Cu inside, Q (100) is high at the same time both crystallite sizes X_s (100) and X_s (111) are large. On the other hand, the outermost surface of upper $HPT_{1/4}$ surface evaluated with the thin-film XRD exhibits high Q (111) and low Q (100) as the same manner. However, the orientation degrees and crystallite sizes for the lower outermost surface of $HPT_{1/4}$ are much different from those of upper surface, these crystallographic discrepancies might be originated from the stiffness of Cu, 40~50 GPa; the upper anvil was fixed, on the other hand, the lower anvil was rotated; an extremely high torsion force between the upper and lower surfaces was applied, *i.e.*, the strong horizontal deformation by the rotating lower anvil.

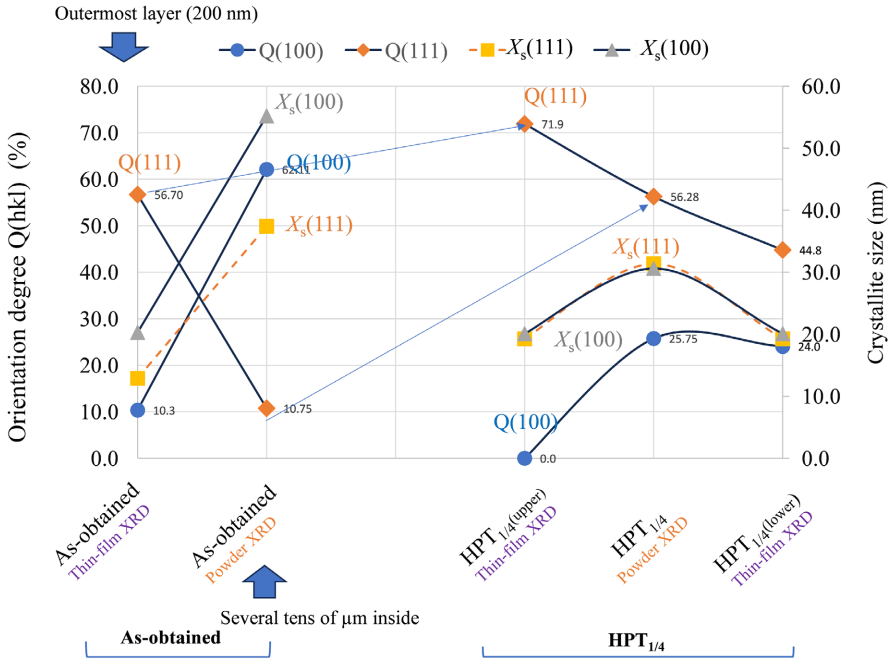

Figure 12. Distribution of orientation degrees; Q (111) and Q (100), and crystallite sizes; X_s(111) and X_s(100), for each (111) and (100) planes, determined using thin-film and powder XRDs, of as-obtained and $HPT_{1/4}$ Cu discs, respectively.

As the CL measurement can present the information about the outermost surface and the fact that in the upper surface there is little evidence for deformation, so in order to investigate the relationship between antibacterial activity through generation of ROS and severe plastic deformation, the surface was polished from the outermost to inside of discs. **Figure 13** shows some properties such as ΣCL (9 min), orientation degrees Q (100), Q (111), and crystallite sizes X_s (100) and X_s (111) as a function of depth from the outermost surface for $HPT_{1/4}$ + DP 523K Cu discs. From these depth profiles, it might be safe that inside of plastic deformed Cu, even after severe HPT, the microstructural change which can introduce the

double thin-oxide layers, *i.e.*, Cu_2O/CuO (as we think that this double thin-oxide layer and their edges can generate ROS in air) in air might decrease with getting deeper. Especially, around 30 to 40 μm in depth, a sudden drop of ΣCL (9 min), corresponding to the "hill" height which was brought by WC (tungsten carbide) grip during HPT process, was observed. The other physical properties are constant until the depth of about 200 μm where ΣCL (9 min) reaches around 20%. These data proved that regardless of the application or not application of severe plastic deformation, only the surface of bulk Cu shows strong antibacterial activity. In summary, although there are numerous publications about the application of severe plastic deformation to control mechanical or functional properties of metallic and non-metallic materials, as discussed in two recent mega-review papers [36] [37], the current study presents the first report on actinobacterial analyses of such materials by the CL method. Since such analyses are quite sensitive to the utmost surface layer of the material, it appears that severe plastic deformation methods not only modify the bulk but also affect the surface properties.

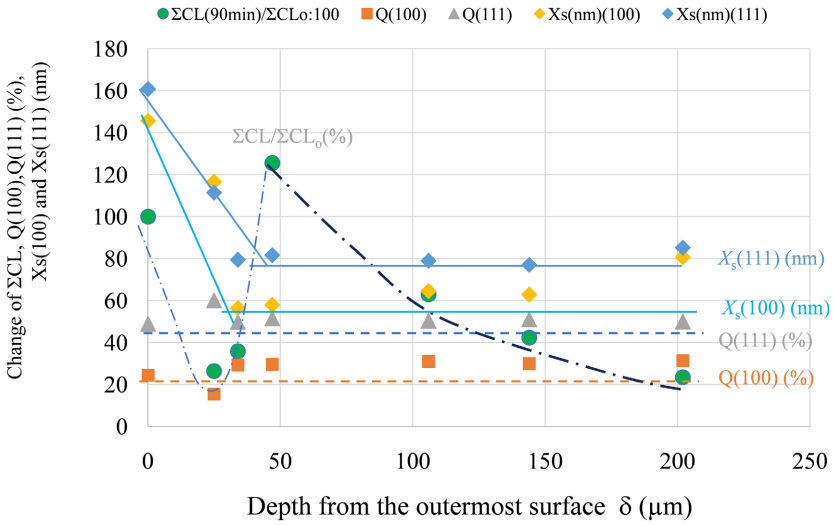

Figure 13. Change of physical properties as a function of depth d from the outermost surface of $HPT_{1/4}$ + DP 523 K for 1.8×10^3 s (30 min).

In summary, although there are numerous publications about the application of severe plastic deformation to control mechanical or functional properties of metallic and non-metallic materials, as discussed in two recent mega-review paperes [36] [37], the current study presents the first report in actinobacterial analyses of such materials by the CL method. Since such analyses are quite sensitive to the outermost surface layer of the material, it appears that severe plastic deformation methods not only modify the bulk also affect the surface properties.

4. Conclusion

Although being much interesting from mechanical and electrical viewpoints, the

antibiotic properties of severely plastic deformed Cu, such as high-pressure torsion (HPT) has not been studied up to now. This paper is the first report about its antibiotic activity using chemiluminescence (CL). From this study following results have been obtained.

About antibacterial activity of HPTed Cu

1) The summation of CL intensity (ΣCL), of Cu disc prepared under the condition of 1/4 round torsion at pressure of 6.0 GPa with a rotating speed of 1.0 rpm, namely $HPT_{1/4}$ Cu disc, increased 2.7 times higher than as-obtained disc.

2) These HPT conditions give the compression rate about 70% - 75% and strain e about 10.

3) Furthermore, a vacuum heating at 523 K for 1.8×10^3 s (250˚C/30 min) brought much higher ΣCL, about 35 times of as-obtained Cu disc.

4) Using the scavenger corresponding to each ROS, about 45% of ROS were strong antibacterial active hydroxy radical × OH and hydrogen peroxide H_2O_2.

Acknowledgements

The authors thank Ms. M. Toda of the Doshisha University Research Centre for Interfacial Phenomena for the laser microscope and SEM observations of the samples.

Conflicts of Interest

The authors declare no conflicts of interest regarding the publication of this paper.

References

[1] ASM Handbook (2005) Forging of Copper and Copper Alloys. In: Semiatin, S.L., Ed., *Metalworking*: *Bulk Forming*, ASM International, 313-317. https://doi.org/10.31399/asm.hb.v14a.a0003997

[2] Lee, I., Bhatta, L., Wu, Y., Daut, L., Figueiredo, R.B., Liss, K., *et al.* (2023) The Cold Angular Rolling Process of Copper Sheets: Unraveling Plastic Deformation Behavior and Unveiling Microstructural Transformations. *Advanced Engineering Materials*, **26**, Article ID: 2300742. https://doi.org/10.1002/adem.202300742

[3] (2025) Copper Stamping Process and Applications. https://www.worthyhardware.com/

[4] Segalina, F. and De Chiffre, L. (2017) Material Testing of Copper by Extrusion-cutting. *Procedia CIRP*, **58**, 375-380. https://doi.org/10.1016/j.procir.2017.03.240

[5] (2018) Copper in the Arts. Copper Development Association Inc.

[6] Shiramoto, K., Mori, A., Watanabe, T. and Hisanabe, K. (2012) Explosive Forming Techniques for Making a Copper Plate Relief. *Science and Technology of Energetic Materials*, **73**, 104-108.

[7] Collini, L. (2012) Copper Alloys—Early Applications and Current Performance—Enhancing Processes. IntechOpen.

[8] Azushima, A., Kopp, R., Korhonen, A., Yang, D.Y., Micari, F., Lahoti, G.D., *et al.* (2008) Severe Plastic Deformation (SPD) Processes for Metals. *CIRP Annals*, **57**, 716-735. https://doi.org/10.1016/j.cirp.2008.09.005

[9] Edalati, K., Fujioka, T. and Horita, Z. (2008) Microstructure and Mechanical Proper-

ties of Pure Cu Processed by High-Pressure Torsion. *Materials Science and Engineering*: *A*, **497**, 168-173. https://doi.org/10.1016/j.msea.2008.06.039

[10] Edalati, K., Imamura, K., Kiss, T. and Horita, Z. (2012) Equal-Channel Angular Pressing and High-Pressure Torsion of Pure Copper: Evolution of Electrical Conductivity and Hardness with Strain. *Materials Transactions*, **53**, 123-127. https://doi.org/10.2320/matertrans.md201109

[11] Ikoma, Y., Matsuda, K., Yoshida, K., Takaira, M. and Kohno, M. (2022) Electric, Thermal, and Optical Properties of Severely Deformed Si Processed by High-Pressure Torsion. *Journal of Applied Physics*, **132**, Article ID: 215101. https://doi.org/10.1063/5.0122826

[12] Fujioka, T. and Horita, Z. (2009) Development of High-Pressure Sliding Process for Microstructural Refinement of Rectangular Metallic Sheets. *Materials Transactions*, **50**, 930-933. https://doi.org/10.2320/matertrans.mrp2008445

[13] Edalati, K. and Horita, Z. (2016) A Review on High-Pressure Torsion (HPT) from 1935 to 1988. *Materials Science and Engineering*: *A*, **652**, 325-352. https://doi.org/10.1016/j.msea.2015.11.074

[14] Torkestani, A. and Dashtbayazi, M.R. (2018) A New Method for Severe Plastic Deformation of the Copper Sheets. *Materials Science and Engineering*: *A*, **737**, 236-244. https://doi.org/10.1016/j.msea.2018.09.054

[15] Rijal, A., Singh, S.P., Han, J., Kawasaki, M. and Kumar, P. (2019) Effect of High-Pressure Torsion on Hardness and Electrical Resistivity of Commercially Pure Cu. *Advanced Engineering Materials*, **22**, Article ID: 1900547. https://doi.org/10.1002/adem.201900547

[16] Hirota, K., Sugimoto, M., Kato, M., Tsukagoshi, K., Tanigawa, T. and Sugimoto, H. (2010) Preparation of Zinc Oxide Ceramics with a Sustainable Antibacterial Activity under Dark Conditions. *Ceramics International*, **36**, 497-506. https://doi.org/10.1016/j.ceramint.2009.09.026

[17] Nguyen, T.M.P., Lemaitre, P., Kato, M., Hirota, K., Tsukagoshi, K., Yamada, H., *et al.* (2021) Preparation of Anatase Titanium Dioxide Nanoparticle Powders Submitting Reactive Oxygen Species (ROS) under Dark Conditions. *Materials Sciences and Applications*, **12**, 89-110. https://doi.org/10.4236/msa.2021.122006

[18] Hirota, K., Tanaka, H., Maeda, T., Tsukagoshi, K., Kawakami, H., Ozawa, T., *et al.* (2023) Evaluation of Reactive Oxygen Species (ROS) Generated on the Surface of Copper Using Chemiluminesence. *Materials Sciences and Applications*, **14**, 482-499. https://doi.org/10.4236/msa.2023.1410032

[19] Wikipedia (2025) Free Encyclopedia, "Antimicrobial Properties of Copper".

[20] Hirota, K., Jinzenji, A., Tsukagoshi, K., Taniguchi, Y., Kawakami, H., Ozawa, T., *et al.* (2023) Antibacterial Activity of Anatase TiO_2 Added Cu Powder. *Journal of the Japan Society of Powder and Powder Metallurgy*, **70**, 121-131. https://doi.org/10.2497/jjspm.70.121

[21] Honkanen, M., Vippola, M. and Lepistö, T. (2008) Oxidation of Copper Alloys Studied by Analytical Transmission Electron Microscopy Cross-Sectional Specimens. *Journal of Materials Research*, **23**, 1350-1357. https://doi.org/10.1557/jmr.2008.0160

[22] Hirota, K., Maeda, T., Tsukagoshi, K., Taniguchi, Y., Kawakami, H., Ozawa, T., *et al.* (2025) Reactive Oxygen Species (ROS) Generated on the Surface of (100)-Plane Grain-Oriented Copper Thin-Film. *Materials Sciences and Applications*, **16**, 27-45. https://doi.org/10.4236/msa.2025.161003

[23] Thermo Fisher Scientific Home. https://www.thermofisher.com

[24] The Chemical Society of Japan (2021) Handbook of Chemistry: Pure Chemistry. 6th Edition, Maruzen-Publishing.

[25] Grass, G., Rensing, C. and Solioz, M. (2011) Metallic Copper as an Antimicrobial Surface. *Applied and Environmental Microbiology*, **77**, 1541-1547. https://doi.org/10.1128/aem.02766-10

[26] Nibur, K.A. and Bahr, D.F. (2003) Identifying Slip Systems around Indentations in FCC Metals. *Scripta Materialia*, **49**, 1055-1060. https://doi.org/10.1016/j.scriptamat.2003.08.021

[27] Muniz, F.T.L., Miranda, M.A.R., Morilla dos Santos, C. and Sasaki, J.M. (2016) The Scherrer Equation and the Dynamical Theory of X-Ray Diffraction. *Acta Crystallographica Section A Foundations and Advances*, **72**, 385-390. https://doi.org/10.1107/s205327331600365x

[28] Wang, P., Bian, Y., Yang, F., Fan, H. and Zheng, B. (2020) Mechanical Properties and Energy Absorption of FCC Lattice Structures with Different Orientation Angles. *Acta Mechanica*, **231**, 3129-3144. https://doi.org/10.1007/s00707-020-02710-x

[29] Kunze, J., Maurice, V., Klein, L.H., Strehblow, H. and Marcus, P. (2004) In Situ STM Study of the Duplex Passive Films Formed on Cu(111) and Cu(001) in 0.1m NaOH. *Corrosion Science*, **46**, 245-264. https://doi.org/10.1016/s0010-938x(03)00140-9

[30] Alipour Tehrani, N., Benoit, M., Dannheim, D., Fiergolski, A., Hynds, D., Klempt, W., *et al.* (2020) Performance Evaluation of Thin Active-Edge Planar Sensors for the CLIC Vertex Detector. *Nuclear Instruments and Methods in Physics Research Section A*: *Accelerators*, *Spectrometers*, *Detectors and Associated Equipment*, **953**, Article ID: 162850. https://doi.org/10.1016/j.nima.2019.162850

[31] Sheng, H., Nakamura, K., Kanno, T., Sasaki, K. and Niwano, Y. (2015) Bactericidal Effect of Photolysis of H_2O_2 in Combination with Sonolysis of Water via Hydroxyl Radical Generation. *PLOS ONE*, **10**, e0132445. https://doi.org/10.1371/journal.pone.0132445

[32] Nasibulin, A.G., Richard, O., Kauppinen, E.I., Brown, D.P., Jokiniemi, J.K. and Altman, I.S. (2002) Nanoparticle Synthesis by Copper (II) Acetylacetonate Vapor Decomposition in the Presence of Oxygen. *Aerosol Science and Technology*, **36**, 899-911. https://doi.org/10.1080/02786820290038546

[33] International Centre for Diffraction Data (ICDD)PDF/JCPDS, Card Number: 04-0836. https://www.icdd.com

[34] Information from Rigaku Holdings Corporation, Tokyo, Japan. https://rigaku-holdings.com

[35] Ledbetter, H.M. and Naimon, E.R. (1974) Elastic Properties of Metals and Alloys. II. Copper. *Journal of Physical and Chemical Reference Data*, **3**, 897-935. https://doi.org/10.1063/1.3253150

[36] Edalati, K., Bachmaier, A., Beloshenko, V.A., Beygelzimer, Y., Blank, V.D., Botta, W.J., *et al.* (2022) Nanomaterials by Severe Plastic Deformation: Review of Historical Developments and Recent Advances. *Materials Research Letters*, **10**, 163-256. https://doi.org/10.1080/21663831.2022.2029779

[37] Edalati, K., Ahmed, A.Q., Akrami, S., Ameyama, K., Aptukov, V., Asfandiyarov, R.N., *et al.* (2024) Severe Plastic Deformation for Producing Superfunctional Ultrafine-Grained and Heterostructured Materials: An Interdisciplinary Review. *Journal of Alloys and Compounds*, **1002**, Article ID: 174667. https://doi.org/10.1016/j.jallcom.2024.174667